

**Freshening over the whole water column as a result of the 2012 subpolar
freshwater anomaly increased the transport of lighter waters of the Irminger
Current between 2014 - 2022**

**Nora Fried¹, Tiago C. Biló^{2,3}, William E. Johns⁴, Caroline A. Katsman⁵, Kristen E.
Fogaren⁶, Meg Yoder⁶, Hilary I. Palevsky⁶, Fiammetta Straneo⁷ and M. Femke de Jong¹**

¹ Department of Ocean Systems, NIOZ, Royal Netherlands Institute for Sea Research, Texel,
Netherlands.

² Cooperative Institute for Marine and Atmospheric Studies, University of Miami, Miami,
Florida, United States

³ Atlantic Oceanographic and Meteorological Laboratory, National Oceanic and Atmospheric
Administration, Florida, United States

⁴ Rosenstiel School of Marine, Atmospheric, and Earth Science, University of Miami,
Florida, United States

⁵ Delft University of Technology, Department of Hydraulic Engineering, Faculty of Civil
Engineering and Geosciences, Delft, Netherlands

⁶ Department of Earth and Environmental Sciences, Boston College, Chestnut Hill,
Massachusetts, USA

⁷ Scripps Institution of Oceanography, University of California San Diego, California, USA

Corresponding author: Nora Fried (nora.fried@nioz.nl)

Key Points:

- Starting in summer 2016, the Irminger Current (IC) freshened over the upper 1500 m until 2018 and stayed fresh until 2022.
- The northward freshwater transport of the IC increased by a factor of 3 from 2014-2015 to 2021-2022.
- As a result, the volume transport of waters lighter than 27.55 kg m^{-3} increased with possible implications for the AMOC's upper limb.

Abstract

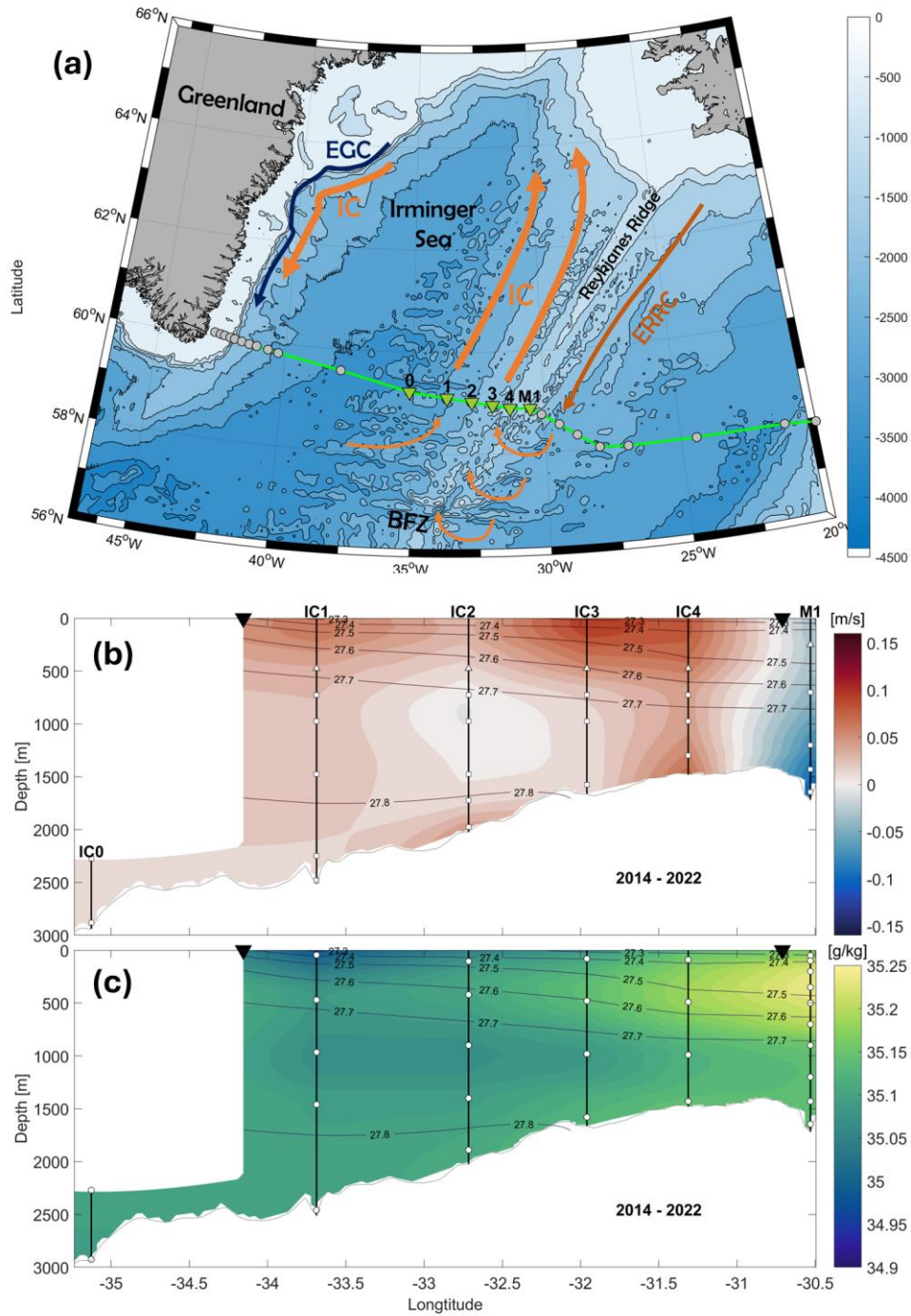
The North Atlantic subpolar gyre experienced strong freshening in recent years starting around 2012. Here, we investigate the imprint of this freshwater anomaly on the water column hydrography and transport variability of the Irminger Current (IC). The IC transports warm and saline waters northward along the western flank of the Reykjanes Ridge as part of the upper limb of the Atlantic Meridional Overturning Circulation (AMOC). To investigate if the salinity anomaly spread and propagated downward, we used high-resolution mooring data from the IC covering the period 2014 – 2022 combined with hydrographic sections from the Irminger Sea and Iceland Basin.

We found that the IC experienced a strong freshening starting in summer 2016. By 2018, this salinity anomaly covers the whole water column down to 1500 m depth and freshened the IC until 2022. In 2022, the IC was at its freshest state observed since the early 1990's.

Hydrographic sections across the adjacent basins showed that the recent freshening spread across the Irminger Sea and was also comparable to its fresh state in the early 1990's. The salinity anomaly increased the freshwater transport of the IC by a factor of three from 2014-2015 to 2021-2022 and caused a decrease in density over much of the water column. This resulted in an increase in the transport of waters lighter than 27.55 kg m^{-3} , potentially strengthening the upper limb of the AMOC.

Plain Language Summary

The subpolar North Atlantic experienced strong freshening in recent years starting around 2012. This paper uses moored observations and hydrographic ship sections to investigate the impact of this freshening on the Irminger Current (IC). The IC brings warm and saline waters northward along the western flank of the Reykjanes Ridge in the Irminger Sea. Between 2014 – 2022, the unusual low surface salinity decreased the salinity of the water column of the IC (and the entire Irminger Sea) down to 1500 m depth. In 2022, the IC was freshest observed since the 1990's, the Irminger Sea was at a similar fresh state as in the early 1990's. In response to the unusual low salinity, the northward transport of fresh waters drastically increased over the 8-year time period. The freshening resulted in an increase of the northward transport of lighter waters by the IC. The observed transport changes in upper ocean waters might impact overturning in the Northeastern Atlantic.

60 **1 Introduction**

61

62 **Figure 1: Schematic overview of the circulation in the Irminger Sea and hydrography of**63 **the Irminger Current (a) Schematic of circulation in the Irminger Sea: Irminger Current**64 **(IC), East Reykjanes Ridge Current (ERRC), East Greenland Current (EGC), Irminger Gyre**65 **(IG) and bathymetric features Bight Fracture Zone (BFZ) and Reykjanes Ridge. Gray dots:**66 **OSNAP East moorings, green triangles: IC array moorings and M1; Green line represents the**

hydrography line **(b)** velocity across IC section from 2014 – 2022 (shading, m s^{-1}) with mean isopycnals (contours); black lines mark mooring locations, white icons mark the depth of ADCPs (triangles) and current meters (squares); black triangles mark IC boundaries; grey line marks bottom topography; **(c)** as (b) but for salinity [g kg^{-1}], here white circles mark the depth of the MicroCATs.

The Atlantic Meridional Overturning Circulation (AMOC) is a major component of the climate system. At the surface, the AMOC is responsible for poleward heat transport. At depth, it transports cold and dense water masses formed by deep convection in the Labrador and Irminger Seas (e.g. Lazier, 1973; Lazier et al., 2001; Marshall & Schott, 1999; Pickart et al., 2003; Pickart and Spall, 2007) and Nordic Seas (e.g. Eldevik et al., 2005; Messias et al., 2008; Våge et al., 2015). Previously, AMOC variability was assumed to be primarily linked to variability in Labrador Sea convection (e.g., Thornalley et al 2018; Yashayaev, 2007; Yeager and Danabasoglu 2014). However, recent studies instead highlight the importance of transformation in the Irminger Sea and Iceland Basin to the AMOC variability in the Subpolar North Atlantic (Fu et al., 2023; Li et al., 2021).

Due to increasing freshwater input and upper ocean stratification in these high latitude regions, climate models predict an AMOC slow down, but uncertainty on the magnitude of the expected AMOC decrease remains large (Fox Kemper et al., 2021). Numerous model studies have shown that the release of large amounts of freshwater for an extended period of time can lead to a partial or complete shutdown of the AMOC (e.g. Jackson and Wood 2018; Jackson et al., 2023; Stouffer et al., 2006). However, intermittent periods of intense freshening of the subpolar North Atlantic on multi-year to decadal time scales have also occurred whose impact on the AMOC remains largely unclear.

From the 1960's to the mid-1990's the North Atlantic experienced several of these transient freshwater anomalies mostly identified signals at the surface. Periods of intense surface freshening, so-called “Great Salinity Anomalies” occurred in the 1970's (Dickson et al., 1988), the 1980's (Belkin et al., 1998) and the 1990's (Belkin, 2004).

The freshening from 1967 – 1971 was one of the strongest low-salinity periods observed in the North Atlantic (Dickson et al., 1988; Kim et al., 2021; Lazier et al., 1980). Earlier studies related the shutdown of Labrador Sea convection to increased stratification due to the low upper ocean salinity (e.g., Gelderloos et al., 2012; Lazier et al., 1980). Alternatively, the recent modeling results from Kim et al. (2021) suggest the reverse: that the 1970's freshening

100 resulted from decreased Labrador Sea convective activity. The authors showed that this
101 convection suppression was mainly driven by weakened atmospheric forcing.
102 The freshening event of the 1990's was followed by a period of increasing salinity (Holliday
103 et al., 2008) up until a new fresh anomaly entered the subpolar gyre in 2012 (Holliday et al.,
104 2020). Due to the increased availability of observations, this most recent salinity anomaly is
105 described in much more detail than earlier events. The decrease in surface salinity could be
106 attributed to changes in wind patterns, which in turn resulted in major changes in the ocean
107 circulation (Holliday et al., 2020). This surface freshening was strengthened by enhanced
108 precipitation due to unusual atmospheric patterns. An important role in the spread of the
109 freshwater anomaly might have been the interaction between the Labrador Current
110 retroflection and the Gulf Stream as recently suggested by Jutras et al. (2023).
111 In this paper, we focus on the fate of this recent surface salinity anomaly in the Irminger Sea,
112 and analyze how it spread over the water column and changed the local hydrography.
113 The hydrography of the subpolar North Atlantic has been observed systematically since 1990
114 with regular repeats of the World Ocean Circulation Experiment AR01E section (WOCE, van
115 Aken et al., 2011) and the Greenland to Portugal OVIDE section (Lherminier et al., 2007;
116 Mercier et al., 2015). Since 2014, AMOC transport in the subpolar gyre has been observed
117 within the basin-wide Overturning in the Subpolar North Atlantic Program (OSNAP, Fu et
118 al., 2023; Li et al., 2021; Lozier et al., 2017, 2019). OSNAP is designed to quantify trans-
119 basin fluxes of volume, heat and freshwater in the subpolar North Atlantic by directly
120 measuring velocity and property fields over the whole water column. The mooring array
121 spans across the Labrador Sea towards Greenland (OSNAP West) and from Greenland
122 towards the Scottish shelf (OSNAP East, grey dots Fig.1a) across the Irminger Sea, the
123 Iceland Basin and Rockall Trough. The overturning at OSNAP appears dominated by its
124 eastern section as first shown by the 2-year time series (Fu et al., 2023; Li et al., 2021; Lozier
125 et al., 2019).
126 In the Irminger Sea, the Irminger Current (IC, Fig.1a) brings relatively warm and saline
127 waters northward along the western flank of the Reykjanes Ridge. It continues cyclonically
128 around the Irminger Sea, flows southward along the east coast of Greenland side by side with
129 the East Greenland Current (EGC) and then turns west into the Labrador Sea at Cape
130 Farewell. Over the Reykjanes Ridge at the OSNAP East line, the IC has a two-core structure
131 with a surface intensified flow and a southward recirculation around 1000 m depth (Chafik et
132 al., 2014; Fried and de Jong, 2022; de Jong et al., 2020; Knutsen et al., 2005; Petit et al.,
133 2019; Sarafanov et al., 2012; Våge et al., 2011, Fig.1b).

As part of OSNAP, a mooring array has been measuring the IC in detail since 2014 (green triangles Fig.1a). The characteristics of the two IC cores have previously been described: the western core is colder and fresher, the eastern core warmer and more saline (Fig.1c, Fried and de Jong, 2022; de Jong et al., 2020; Petit et al., 2019; Våge et al., 2011). At OSNAP East, Fried et al. (2023) identified two main source regions for the two IC cores using a Lagrangian model study: the central Irminger Sea and the Iceland Basin. The western core mostly originates from the central Irminger Sea with a smaller contribution from the Iceland Basin. The eastern core instead has a clear connection to the Iceland Basin and contains a smaller contribution from the central Irminger Sea. In this paper, we investigate the spread of the salinity anomaly with respect to both basins.

Based on the 2014-2016 time series, de Jong et al. (2020) showed that the mean volume transport in the two IC cores is nearly equal, but that IC the variability is dominated by the variability of its western core. The warmer and more saline, eastern core is responsible for most of the northward heat and salt transport within the array. De Jong et al. (2020) find a mean transport of 10.6 ± 1.4 Sv (std error) for the whole IC at OSNAP East. Variability of the total volume transport is high with a standard deviation of 9.2 Sv (daily values) and 4.4 Sv from monthly values. The 2014-2016 time series showed a mean freshwater transport of -22.5 mSv (de Jong et al., 2020). This negative value of the freshwater transport reflects that the IC is more saline than the reference salinity used to calculate freshwater transports from the OSNAP observations (de Jong et al., 2020) and, in the mean, brings salt northward. Negative freshwater transport can therefore be interpreted as positive northward salt transport.

Since 2016, the IC and the Irminger Sea in general have freshened considerably. The initial arrival of the fresh anomaly was described by de Jong et al. (2020). They show that the anomaly arrived in summer 2016 in the near surface layer of the easternmost IC mooring. The arrival and impact of the surface fresh anomaly in the central Irminger Sea was investigated by Biló et al. (2022). They emphasize that the salinity anomaly resulted in fresher convective waters in 2017-2018 and that it contributed to suppressing the convection in the following winters. Here, we will show that, since then, the anomaly has transitioned from a near surface anomaly to a general freshening of the entire water column which may have implications on the basin-wide density structure and AMOC transport.

This paper is organized as follows: Section 2 introduces the mooring data and hydrographic sections as well as the data processing steps. Section 3 discusses the downward propagation

168 and spread of the salinity anomaly at the mooring array throughout the 8-year record. Section
169 4 puts the decreasing salinity into perspective of changes in the whole Irminger Sea and
170 Iceland Basin and compares it to salinity changes in the Irminger Sea over a 30-year time
171 period. Section 5 links the decrease in salinity to the density structure and transport
172 variability of the IC. The strong decrease in salinity at the IC array will be discussed with
173 respect to literature in section 6.

2 Data and Methods

2.1 The Irminger Current mooring array

In July 2014, the Royal Netherlands Institute for Sea Research (NIOZ) first deployed five moorings on the western flank of the Reykjanes Ridge to directly measure the transport of the IC. The moorings were deployed as part of OSNAP and belong to its sub-section OSNAP East. Here, we analyze the full 8-year time series that is available up to July 2022.

The NIOZ mooring array consists of four long (IC1, IC2, IC3, IC4) and one short mooring (IC0) within the two-core structure of the IC (Fig.1a, b). To determine the boundary between the southward flow of the East Reykjanes Ridge Current (ERRC) and the northward flow of the IC, we include the tall mooring M1 on the eastern side of the Reykjanes Ridge in our analysis. M1 is maintained by the University of Miami. The four long moorings reach from the bottom up to ~60 m below the sea surface and measure velocity, temperature and salinity. The moorings are equipped with upward looking ADCPs (Acoustic Doppler Current Profiler, RDI 75 kHz Long Ranger) and single point current meters (CM, either Aanderaa RCM11 or Nortek Aquadopps) to measure the velocity field. We use Sea-Bird Electronics SBE37 (MicroCATs) and Sea-Bird Electronics SBE56 (thermistors) to measure temperature and salinity. The short mooring IC0 only covers the lower 700 m of the water column and is equipped with MicroCATs and CMs only. The M1 mooring has an upward-looking ADCP, Nortek Aquadopp current meters and MicroCATs (see Koman et al., 2020 for additional information on the set-up of that mooring). Sampling rates are 1 hour for the ADCPs, 30 minutes for the CM, 15 minutes for the MicroCATs, and 5 minutes for the thermistors.

2.2 Mooring Data Processing

All data processing consistently involved the following steps. First, the data were low-pass filtered with a 41-hr Butterworth filter to remove tides and inertial motion and subsampled on a daily grid. Next, all profiles were vertically interpolated with the MATLAB “pchip” function and horizontally interpolated linearly on a grid with bottom following contours. The IC flows in a north-east direction along the ridge with an angle to the mooring array. To be able to compute transports across the array we rotate the velocities clockwise by 10° as a third step. The resulting velocities are now aligned with the orientation of the array line and approximately with the main flow direction.

After filling the data gaps we obtain daily fields of along- and across-stream velocity, potential temperature and practical salinity from 2014 - 2022. Finally, we convert the

observed potential temperature and practical salinity to conservative temperature and absolute salinity using TEOS-10 (McDougall & Parker, 2011). Yearly means described in the text are computed from summer to summer (1st of August – 31st of July). A detailed description on data processing can be found in de Jong et al. (2020) and Fried et al. (2022).

2.3 Volume, heat and freshwater transport

From the mooring data we calculated volume, heat and freshwater transports following de Jong et al. (2020) and Fried and de Jong (2022). Volume transport estimates are derived from the daily fields. The total volume transport V is defined as:

$$V = \int_{X_w}^{X_e} \int_{Z_{max}}^0 v(x, y, t) dz dx \quad [Sv = 10^6 \text{ m}^3 \text{ s}^{-1}], \quad (1)$$

where v is across-array velocity, X_w and X_e are the western and eastern boundaries respectively (indicated by black triangles in Figure 1b, c), the surface (0) and bottom (Z_{max}). We define the IC transport between 34.1°– 30.7°W (black triangles Fig. 1b, c) following Våge et al. (2011).

We calculated the heat transport H with respect to a reference temperature $T_{ref} = 0^\circ\text{C}$ using:

$$H = \rho c_p \int_{X_w}^{X_e} \int_{Z_{max}}^0 v(x, y, t) (T(x, y, t) - T_{ref}) dz dx \quad [PW = 10^{15} \text{ W}], \quad (2)$$

where ρ is density and c_p is the specific heat capacity. Density and specific heat capacity are calculated respectively per time step from the gridded fields using TEOS-10 (McDougall & Parker, 2011).

The freshwater transport F is defined as:

$$F = \int_{X_w}^{X_e} \int_{Z_{max}}^0 v(x, y, t) \left(1 - \frac{S(x, y, t)}{S_{ref}} \right) dz dx \quad [\text{mSv}]. \quad (3)$$

We use the reference salinity $S_{ref} = 34.9189 \text{ g kg}^{-1}$ (compare de Jong et al., 2020). As the IC has a higher salinity this results in negative freshwater transport.

To investigate the transport changes in different parts of the water column, we compute the transports for three different density classes. We use the potential density σ_0 (hereafter interchangeably referred to as density for simplicity) of maximum overturning in OSNAP 27.55 kg m^{-3} as a separation between upper and lower AMOC density classes (Fu et al., 2023; Li et al., 2021). Additionally, we define waters denser than 27.8 kg m^{-3} as overflow waters. Hence, we have three layers: from the surface to 27.55 kg m^{-3} (Layer 1), between $27.55 - 27.8 \text{ kg m}^{-3}$ (Layer 2) and below 27.8 kg m^{-3} (Layer 3).

2.4 Hydrographic sections at OSNAP East

To quantify the hydrographic changes the Irminger Sea underwent within the last 30 years we use temperature and salinity from CTD stations. We use hydrographic sections across the Irminger Sea and the Iceland Basin along the WOCE AR01E repeat sections (van Aken et al., 2011) and the Greenland to Portugal OVIDE section (Lherminier et al., 2007; Mercier et al., 2015). The AR01E section aligns with the OSNAP East line and therefore allows us to link changes at the IC mooring array to basin-wide changes over a longer time period. This section has been observed with ships since 1990, nearly every year, mostly in summer. For the 2022 occupation of the OSNAP East section, dissolved oxygen was measured using a SBE43 sensor and calibrated using discrete water samples measured for oxygen using shipboard Winkler titrations.

All section data was vertically interpolated to a regular 1 m depth grid. To account for the unequal amount of CTD stations per year, we created a grid along the OSNAP East section with 0.1° resolution in the horizontal. The data was put to the nearest grid point and then interpolated horizontally. From the 6 sections between 2014-2022 we compute an OSNAP mean section (referred to as “OSNAP mean”).

To put recent salinity changes into a long-term perspective we specifically focus on two sections both taken in September: 1992 and 2005. Those two years best mark the extreme variability in the Irminger Sea in the past 30 years. In 1992 the Irminger Sea was freshest and in 2005 most saline. To compare changes in the IC’s salinity between different years, we create mean vertical profiles of salinity for the IC between 34.1° - 30.7° W (black triangles Fig.1b,c).

3. Salinity changes in the Irminger Current

To understand the changes within the IC, and consequently changes of the AMOC's upper limb, we first investigate the spread of the near surface salinity anomaly over the whole water column across the IC mooring array between 2014 – 2022.

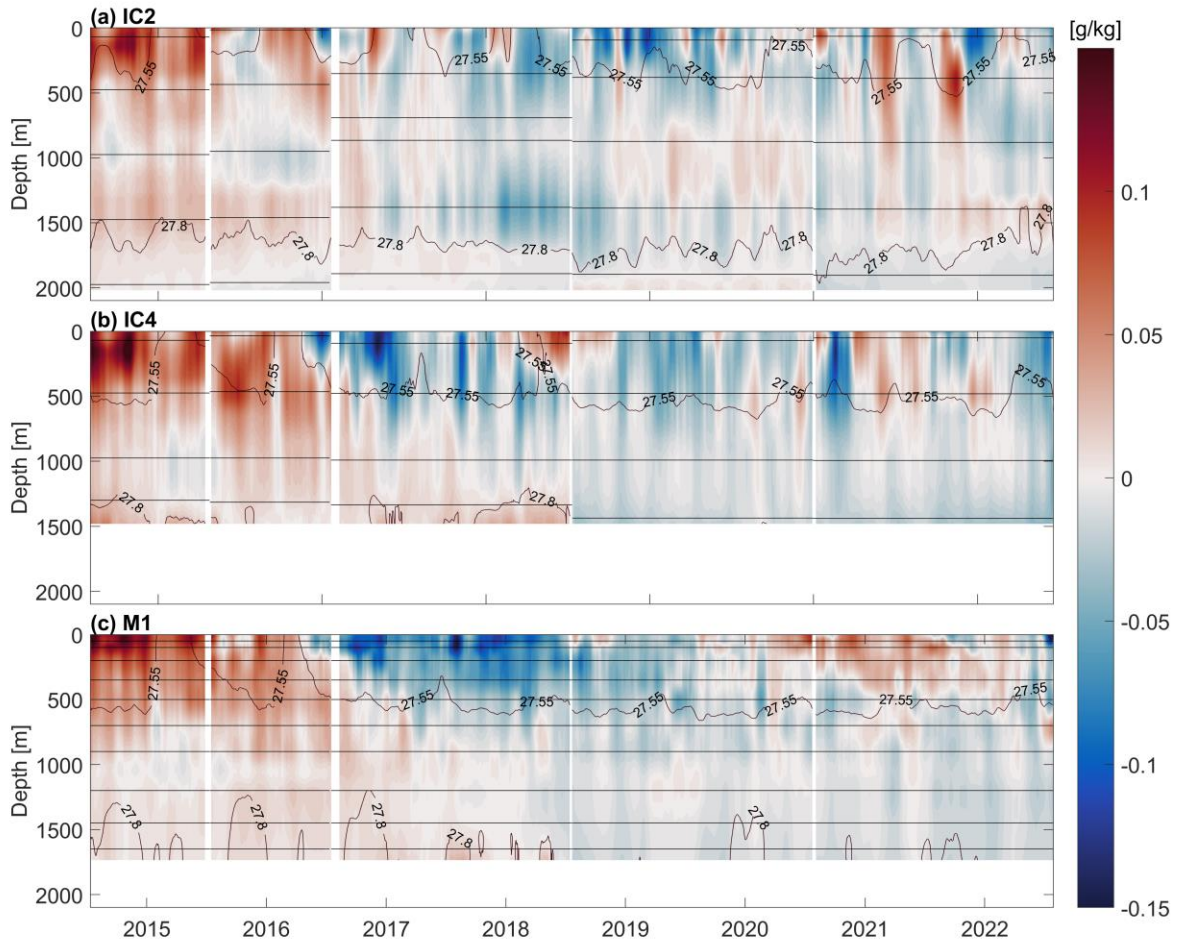


Figure 2: Salinity evolution at IC2, IC4 and M1 Daily salinity anomalies from IC2 (a), IC4 (b) and M1 (c) mooring (shading) overlaid with potential density (contours). The anomalies are computed by removing the 2014-2022 mean salinity and seasonal cycle at each location and depth. Horizontal black lines mark instrument depths for respective deployment periods.

The recent salinity anomaly described by Holliday et al. (2020) circulated in the eastern subpolar gyre between 2012 and 2016. We highlight the arrival and deepening of this freshening signal at the IC moorings by showing the salinity anomaly with respect to the 8-year mean salinity (Fig.2). Throughout the year, the IC is more saline in summer and fresher

in winter. Figure 2 shows the salinity anomalies from IC4 (Fig.2b), located in the most saline waters of the IC over the top of the Reykjanes Ridge, and from IC2 (Fig.2a), located on the edge of the saline waters ($\sim 35 \text{ g kg}^{-1}$) and near the western edge of the eastern IC core (Fig.1b,c). For a comparison of the arrival of the salinity anomaly in the Irminger Sea we additionally show M1 located on eastern side of the Reykjanes Ridge.

The onset of the negative salinity anomaly in the upper 300m at the moorings is around summer 2016. At IC4, the anomaly gradually extends over more of the water column through 2017-2018 and is seen at depths down to 1500m by summer 2018. The anomaly is stronger at IC4. At IC2, the anomaly appears over the whole water column in winter 2017/2018. IC2 shows more short-term variability overlaying the interannual signal.

There is an overall decrease in density associated with the freshening of the water column at all moorings (Fig.2). As a result, the isopycnal of maximum subpolar overturning (i.e., $\sigma_0=27.55$) deepens due to intense freshening near the surface. While this isopycnal was outcropping during winter in 2014 and 2015, it stays well below 300 m after summer 2018 until the end of the deployment. Additionally, the deep isopycnal defining the overflow waters (i.e., $\sigma_0=27.8 \text{ kg m}^{-3}$) retreats offshore, away from the top of the ridge, disappearing from the IC4 records in 2018. The evolution on the eastern side of the ridge at M1 is very similar to IC4, highlighting the connection of the two moorings.

To get a better sense of the temporal and spatial evolution of the salinity over the whole IC, we now focus on yearly mean anomaly sections from the moorings with respect to the 8-year mean salinity shown in Figure 1c. Figure 3a reveals that the year 2014-2015 was by far the most saline year in the 8-year record. Especially the upper 500 m show a strong positive anomaly across the whole array compared to the 8-year mean (0.09 g kg^{-1}). The positive salinity anomaly is weaker in 2015-2016 (Fig.3b). In 2016-2017, with the arrival of the fresh anomaly, a negative salinity anomaly becomes visible in the upper 500m, most pronounced between IC4 and M1 (-0.06 g kg^{-1} , Fig.3c). In 2017-2018, the anomaly deepens in the middle of the array. Slight positive anomaly remains at IC1 below 1000m and at IC4 (0.01 g kg^{-1} , Fig.3d). By 2018-2019, the negative salinity anomaly covers the whole array, but its amplitude is weaker as the signal is gradually diluted most likely due to vertical mixing (-0.01 - -0.05 g kg^{-1} , Fig.3e). Between 2019-2021 (Fig.3f,g) the anomaly weakens even further. Some saline waters reappear resulting in slight positive anomalies in the eastern part of the array. In 2021-2022, fresher waters appear in the upper 300m again, which decreases the salinity ($\sim -0.03 \text{ g kg}^{-1}$), particularly at the surface at IC1.

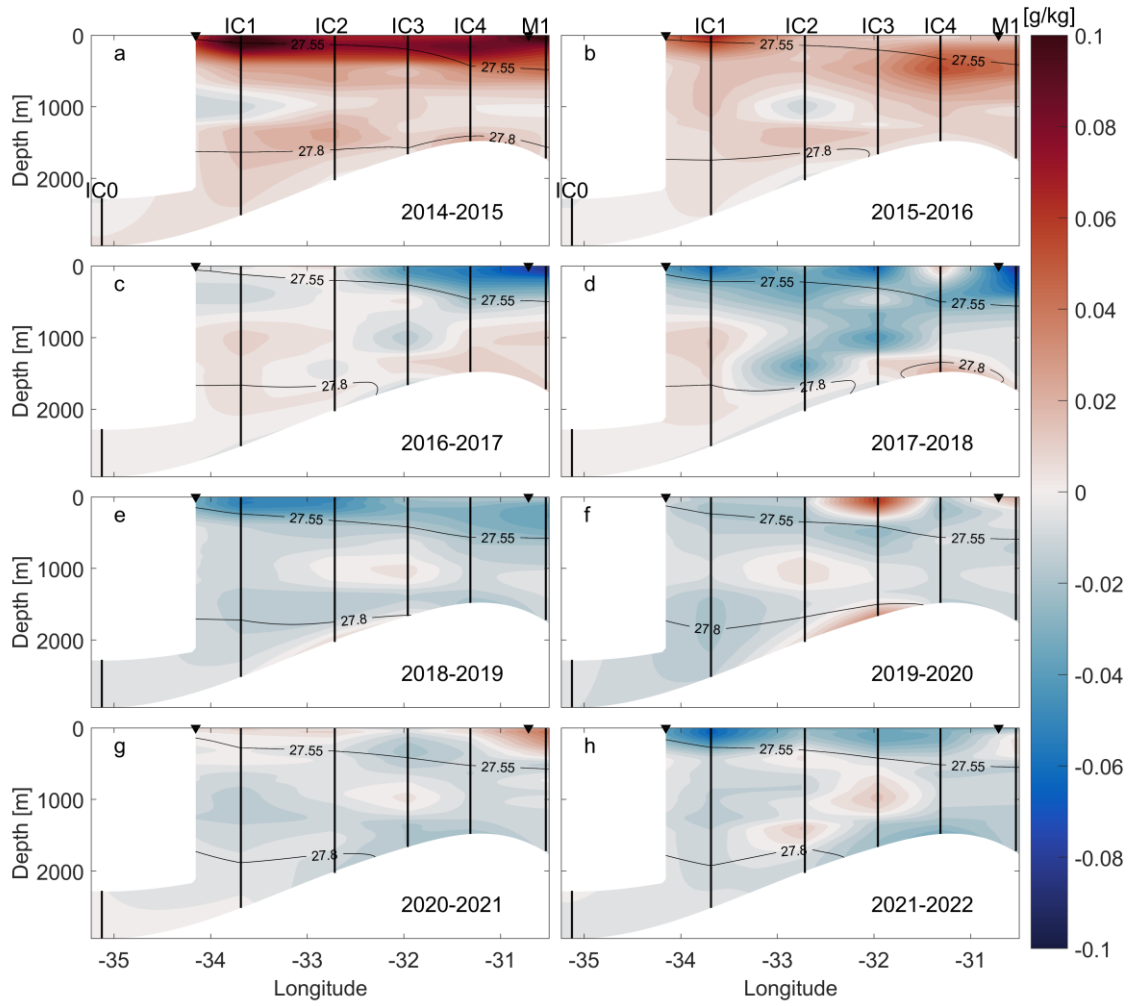


Figure 3: Annual mean salinity anomalies for IC array from 2014-2022 Salinity anomalies from summer – summer for the IC referenced to the mean salinity over 2014 - 2022 (color) with yearly mean isopycnals. Black triangles at the surface mark the IC boundaries. Black vertical lines mark the mooring locations.

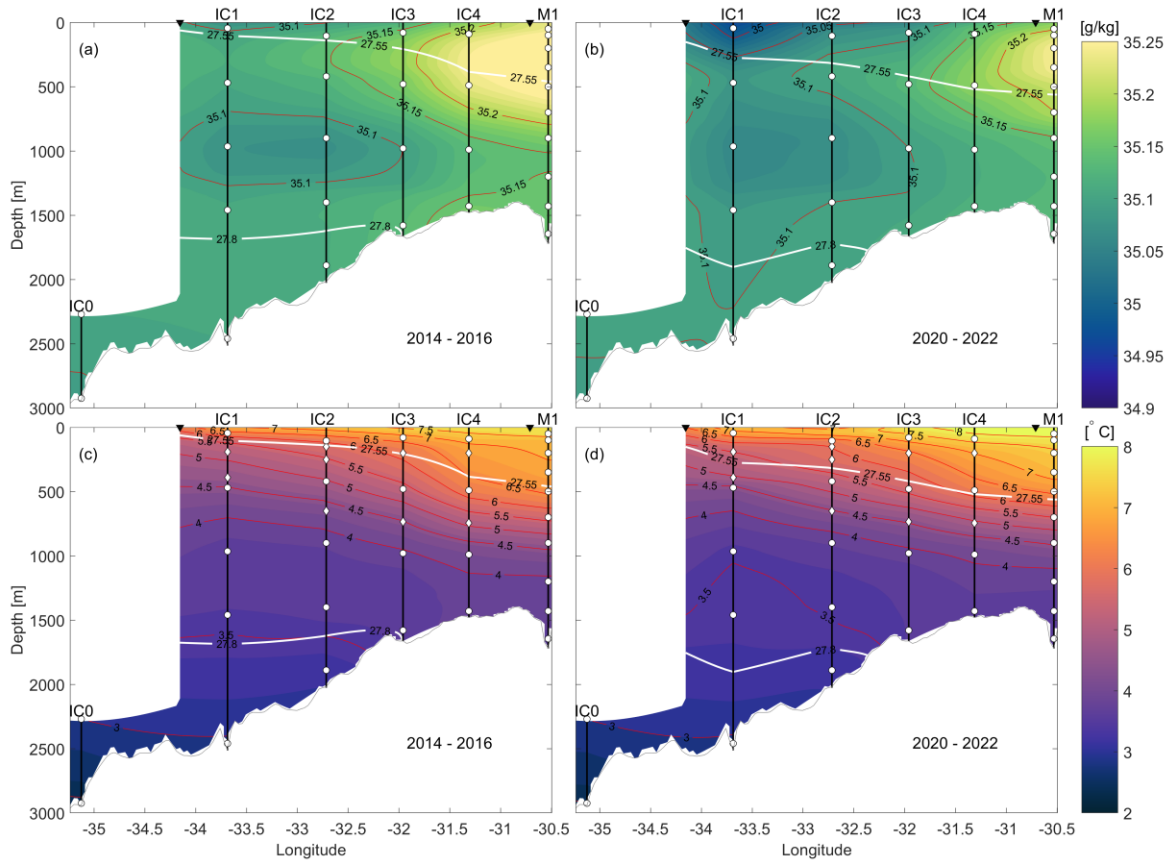


Figure 4: Two-year mean absolute salinity and conservative temperature at IC array
(a,b) Mean salinity for (a) 2014-2016 and (b) 2020-2022. Isohalines with a 0.1 g kg^{-1} interval are depicted in red. The $\sigma_0 = 27.55$ and 27.8 kg m^{-3} - isopycnals are indicated by white contours. Black triangles at the surface mark the IC boundaries. Moorings are marked with black vertical lines (IC0-IC4, M1) and MicroCAT depths are denoted by white circles. Grey line marks the bottom topography. **(c,d)** as (a,b) but for mean conservative temperature (color). Isotherms with a 0.5°C interval are depicted in red. Thermistors are marked with white diamonds.

To further contrast the extreme changes in absolute salinity and highlight the role of salinity in the density changes, we show the salinity and temperature changes from two periods: 2014-2016 and 2020-2022 (Fig.4).

The salinity decreased over the entire water column of the IC section and dominated the changes in density over changes in temperature. The first two years, 2014-2016, were characterized by a very saline IC with absolute salinities higher than $S = 35.15 \text{ g kg}^{-1}$ in the upper 500m (Fig.4a). The $S = 35.15 \text{ g kg}^{-1}$ isohaline extended west nearly to the location of

IC2 (Fig.4a). In 2020-2022, this isohaline is found further east between IC3 and IC4 (Fig.4b). In addition, the volume of water with salinity below 35.1 g kg^{-1} expands from an initially ~500m thick layer at IC1 and IC2 to filling most of the water column at IC1 and IC2 at the end of the record. The near bottom salinity maximum at IC3 and IC4 associated with Icelandic Slope Water is much reduced compared to 2014-2016 (van Aken & de Boer, 1995; Johns et al., 2021; Read, 2000).

The expansion of the low salinity volume in layers deeper than 1000 m is accompanied by a slight cooling (Fig.4c,d). The depth of the 3.5°C -isotherm decreased by 500m in 2020-2022 compared to 2014-2016. In contrast, the uppermost eastern waters are slightly warmer in 2020-2022, resulting in the 7°C -isotherm at IC4 moving down by 100m by 2020-2022.

Overall, we find a decrease in density. Freshening dominates over the cooling in deeper layers. The upper eastern waters got both fresher and warmer adding to the decrease in density.

To sum up, we showed that density changes at the IC array between 2014-2022 were dominated by the decreasing salinity.

4 Salinity changes in the Irminger Sea and Iceland Basin

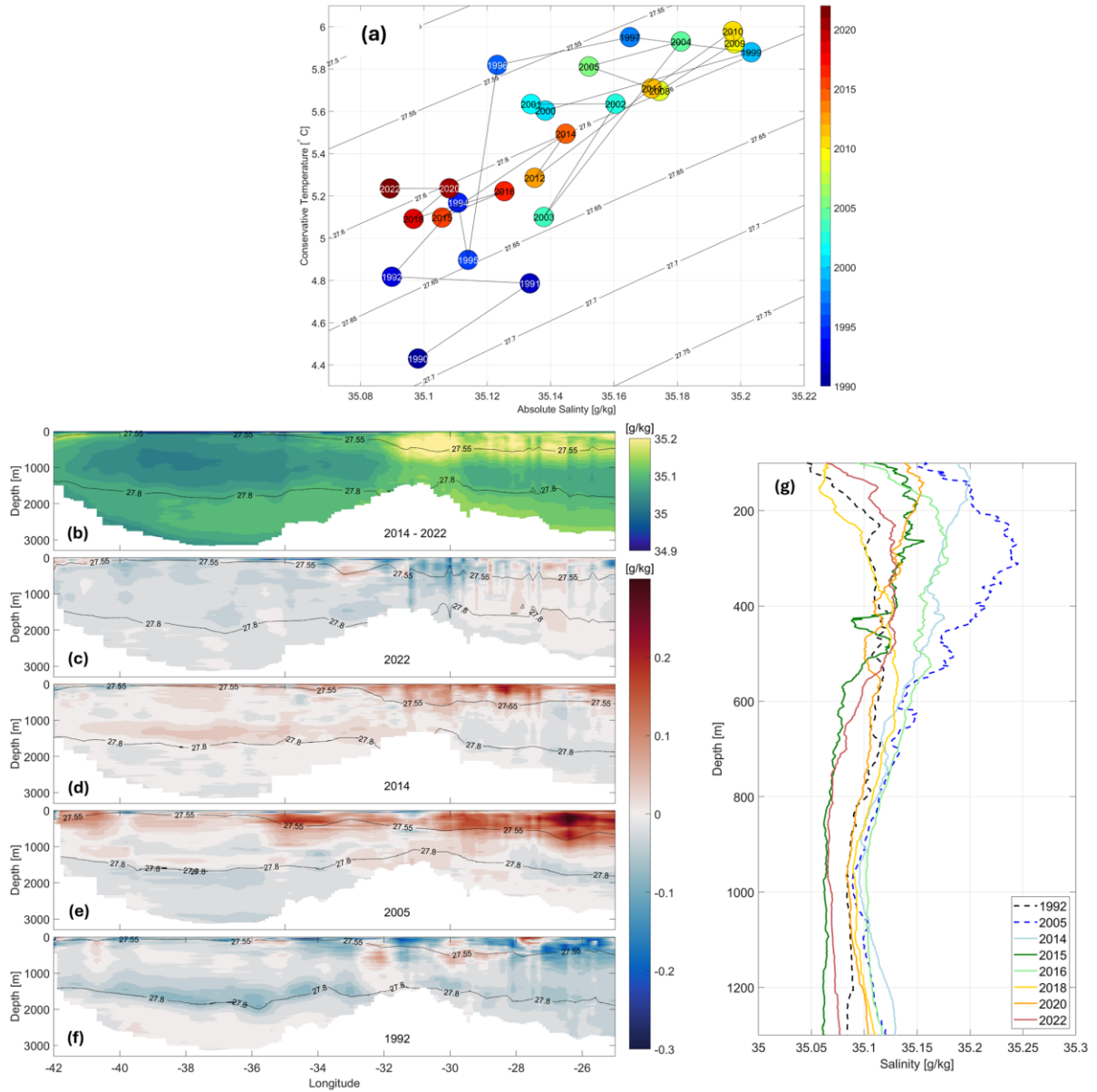


Figure 5: Salinity at OSNAP East section with salinity profiles for the IC (a) TS-diagram of the upper 1000m in the Irminger Current from hydrographic section between 1990 – 2022. Average absolute salinity and conservative temperature from for the IC between the IC boundaries and the main core of the IC up to 1000m depths from all available ship sections. (b) mean salinity from hydrographic sections between 2014 – 2022 (color) with isopycnals (contours); (c-f) salinity anomaly compared to (a) with mean isopycnals for each year (contours) for 2022, 2014, 2005 and 1992. (g) IC salinity profiles averaged between 34.1°-30.7°W for all hydrographic sections during the OSNAP time period (solid, colored lines) and 1992 and 2005 (dashed lines).

In the following, we investigate the spatial extend of the freshening signal. Since we have a long observational record of salinity from hydrographic sections, we can put the changes in the IC into the perspective of changes in the Irminger Sea and Iceland Basin.

In Figure 5, we compare the salinity changes found at the IC array to changes along the whole AR01E section from single summer snap-shots using hydrographic sections. We focus on the most recently collected section at OSNAP East from 2022, which exhibited the most widespread salinity anomaly at the IC array, and 2014 which was most saline (Fig.3a, h). In addition, we compare this to the years 2005 and 1992 which both mark extreme years in salinity in the Irminger Sea and Iceland Basin. In Figure 5a we show a mean TS-diagram of the upper 1000 m of the IC from 25 CTD sections between 1990 and 2022. The years 1992 and 2005 contrast the fresh state of the 1990's with the very warm and saline mid-2000's (Fig.5a). Over the whole array 2005 shows the strongest anomaly. For interpretation it is important to keep in mind that sections are not fully synoptic and that the anomalies we describe propagate around the basin, peaking at different times in different regions.

The OSNAP mean from 2014-2022 (Fig.5b) exhibits higher salinities in the Iceland Basin compared to the Irminger Sea, where most saline waters can be found at the top of the Reykjanes Ridge. In the central Irminger Sea, we find low salinity waters typically known as Labrador Sea Water. Those waters were either formed in the Labrador Sea and exported to the Irminger Sea or formed by local convection in the Irminger Sea itself (de Jong et al., 2012, 2018; de Jong & de Steur, 2016; Piron et al., 2016). The 27.55-isopycnal exhibits a strong slope in the vicinity of the IC, marking its strongest horizontal pressure gradients and velocities.

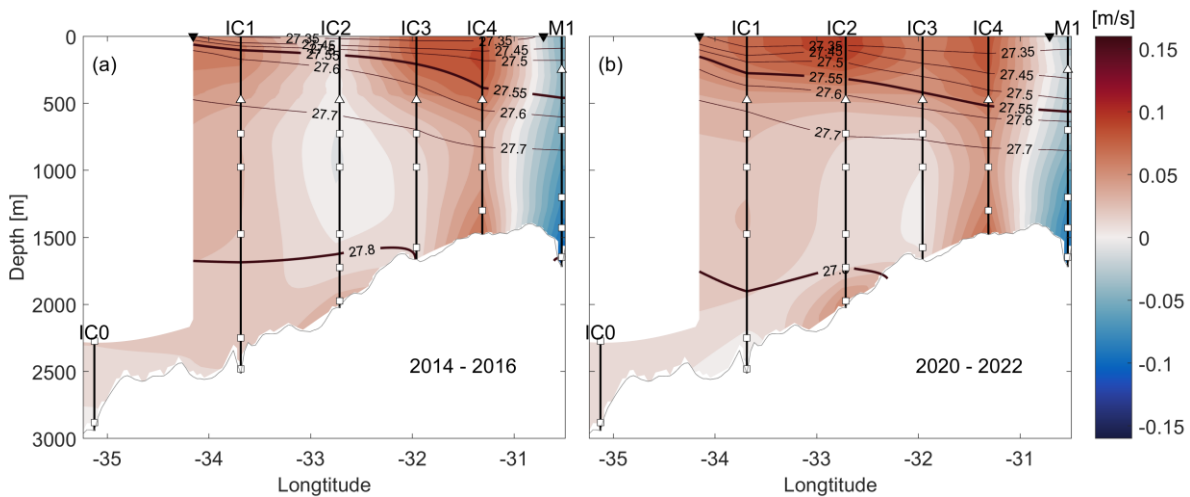
In 2022, most of the section shows a negative salinity anomaly (-0.01 g kg^{-1} , Fig.5c). The decrease in salinity is strongest over the Reykjanes Ridge (-0.1 g kg^{-1}), where typically the most saline waters in this section are found (Fig.5b). While waters below 300m in the Iceland Basin are more saline, the Irminger Sea is slightly fresher than the mean. The freshening in 2022 is especially obvious when comparing it to 2014. Fig.5d shows that the positive salinity anomaly is not limited to the IC but extends across the Irminger Sea and the Iceland Basin, where the upper 700m show a positive salinity anomaly (0.1 g kg^{-1}). Below, in the layers associated with Labrador Sea Water, the Iceland Basin is fresher (-0.002 g kg^{-1}). The Iceland Basin shows a negative salinity signal below 700m.

Changes observed at the IC mooring array do extend into the Irminger Sea. But are these changes associated with the recent salinity anomaly exceptional? Long-term hydrographic changes in the central Irminger Sea are described by van Aken et al. (2011) and de Jong et al. (submitted). They identified the early 1990's as the freshest period in the record since 1950. At the IC, the 2005-section exhibits a thin fresh summer layer at the surface that results in a slightly fresher TS-mean for the IC (Fig.5a, Fig.5e). In 2005, the upper 1000m exhibit a positive salinity anomaly, strongest in the Iceland Basin (Fig.5e). Note that the ISOW layer is also saltier than average, probably because of the rapid entrainment of saline Atlantic waters in the ISOW plume (e.g., Devana et al., 2021; Chafik & Holliday, 2022). In the Irminger Sea instead, the waters below the 27.8 kg m^{-3} -isopycnals waters are fresher. In 1992, all waters masses at the entire section experienced a freshening (Fig.5f), which is stronger than in 2022. Especially the Iceland Basin is very fresh compared to the OSNAP mean. Holliday et al. (2020) showed that the most recent salinity anomaly peaked in 2016-2017 in the Iceland Basin. By 2022, the anomaly in the Iceland Basin has diluted and weakened and therefore appears less strong.

To investigate the stratification of the IC, Fig.5g shows vertical salinity profiles. The 1992 profile (black dashed line in Fig. 5g) shows very little stratification in salinity, the result of deep convective mixing in preceding winters. Deep convection ceased around 1995, and a period of predominantly weak winters lasted until 2007 (de Jong et al., (submitted)). During the late 1990's and early 2000's the basin slowly restratified with warmer, more saline water. The 2005 profile (blue dashed line in Fig. 5g) shows a salinity minimum at 1000 dbar, a remnant of convective waters, with strongly increasing salinity profile upwards to around 300 dbar. These upper waters are the warm, saline waters with an IC origin. A thin fresher layer is found at the top, typical for summer stratification (Sterl & de Jong, 2022). Below 100 m, the IC is most saline compared to the OSNAP years and 1992. Since 2005, there has been intermittent convection until the winter of 2014 – 2015, but not strong enough to halt the seasonal restratification of the basin (de Jong et al., submitted). Exceptionally strong convection event occurred in the winters of 2014-2015 and 2015-2016 (de Jong & de Steur, 2016; de Jong et al., 2018). The 2014 (summer) profile shows the salinity of the water column before that event. It shows that most of the water column had become more saline than the 2005 profile, except for the 200-500 dbar layer. The 2015 profile instead is much fresher, especially above the recorded mixed layer depths (~1500 dbar), except for the uppermost layer. The 2016 profile got even more saline throughout the water column except

for the upper 200 m. The freshening near the surface marks the onset of the salinity anomaly. The section was taken in August 2016 which goes in line with the onset of the salinity anomaly observed by our moorings. The 2018 profile in turn is much fresher in the upper 600 meters. Between 150-250 m the 2018 profile is even fresher than the profile from 1992. The 2020 profile shows that salinity in the upper 300 m increased again. In 2022, the waters above 250 m freshened. At depth, below 500 m, the downward mixing of the salinity anomaly made the IC even fresher than in 1992.

The recent freshening at the IC array is comparable to the fresh state in the early 1990's. While the surface freshening is comparable to 1992, the waters below 500 m are about 0.03 g kg^{-1} fresher in 2022 than in 1992. From the IC, the anomaly spread into the entire Irminger Sea over upper 1500 m. The freshening is comparable to the fresh state in the 1990's with the anomaly peaking in 2016-2017 in the Iceland Basin and in 2018-2019 in the Irminger Sea.



5 Changes in the Irminger Current's velocity structure and transports

Figure 6: Across-section velocities at IC array (a, b) Mean velocity across array for (a) 2014 – 2016 and (b) 2020 – 2022. The isopycnals are indicated by black contours. Black triangles at the surface mark the IC boundaries. Moorings are marked with black vertical lines (IC0-IC4, M1). Blue (red) shading mark southward (northward) velocities. Current meters and ADCPs are marked with white boxes/triangles respectively. Grey line marks the bottom topography.

To understand potential changes in the AMOC's upper limb in response to the recent freshwater anomaly, we investigate the implications of the observed salinity and density changes on the velocity structure of the IC and its transport.

As shown in Figure 4 the strong changes in salinity were not compensated by strong changes in temperature. Therefore, resulting changes in the density structure can primarily be attributed to the salinity anomaly. The changes in salinity in turn could potentially have affected the velocity structure of the IC by changing the slope of the isopycnals and with that the location of strongest velocities (Fig.6a,b). In addition to a change in the density field the changing velocity could also be related to other factors like winds that were not investigated in this study. The 2014-2016 mean displays a clear two-core structure separated by a very weak southward recirculation at intermediate depth. In 2020-2022, the western core moved closer to the eastern core and the southward flow around IC2 at 1000m depth disappeared (Fig.6b). The region below 1500 m at IC3 is still characterized by low velocities. Maximum velocity in the upper layer increased compared to 2014-2016 for both cores. Comparing the mean depth of the two chosen isopycnals (27.55 kg m^{-3} , 27.8 kg m^{-3}), both have deepened by 2020-2022. Waters denser than the 27.8 kg m^{-3} -isopycnal are no longer seen at IC3 at the end of the record.

Lastly, we present the imprints of the salinity anomaly on freshwater, heat and volume transport of the IC (Fig.7). All correlations shown in the following are statistically significant on a 95% confidence interval. At the IC, the northward freshwater transport is negative because the salinity of the IC is higher than the reference salinity (Equation 3). A negative freshwater transport means the northward transport of salt by the IC. For a better visualization of the saline IC, we reverse the axis for freshwater transport (Fig.7) to represent a decrease or increase in salinity more intuitively. A minimum (maximum) in freshwater transport represents a decrease (increase) in northward salt transport. The mean freshwater transport over the 8-year time series is $-8.1 \pm 13.0 \text{ mSv}$.

The freshwater transport drastically changed from -16.1 mSv in 2015-2016 to -6.1 mSv in 2016-2017(Fig.7a, Tab.1) with the arrival of the salinity anomaly at the IC array. Those numbers indicate the diminishing northward salt transport by the IC that reached its minimum in 2017-2018. From 2018-2019 onwards, the northward salt transport recovers but remains lower than at the start of the record.

476 The IC heat transport shows a different evolution than freshwater transport (red line in Fig.7a,
477 Tab.1). Both time series are anti-correlated with $r=-0.37$. Clearly, the correlation between
478 heat and freshwater transport changes throughout the observed time period (Fig.7a). We find
479 a strong correlation between heat and freshwater transport before the arrival of the salinity
480 anomaly until 2016 ($r=-0.79$), after which the correlation decreases to $r=-0.22$. This
481 highlights the impact the salinity anomaly has on the freshwater transport. Throughout the
482 eight years, the heat transport is strongly correlated to volume transport (black line Fig.7d,
483 $r=0.98$) and increased associated with the increasing velocities and the slight warming of the
484 waters in the upper east of the array.

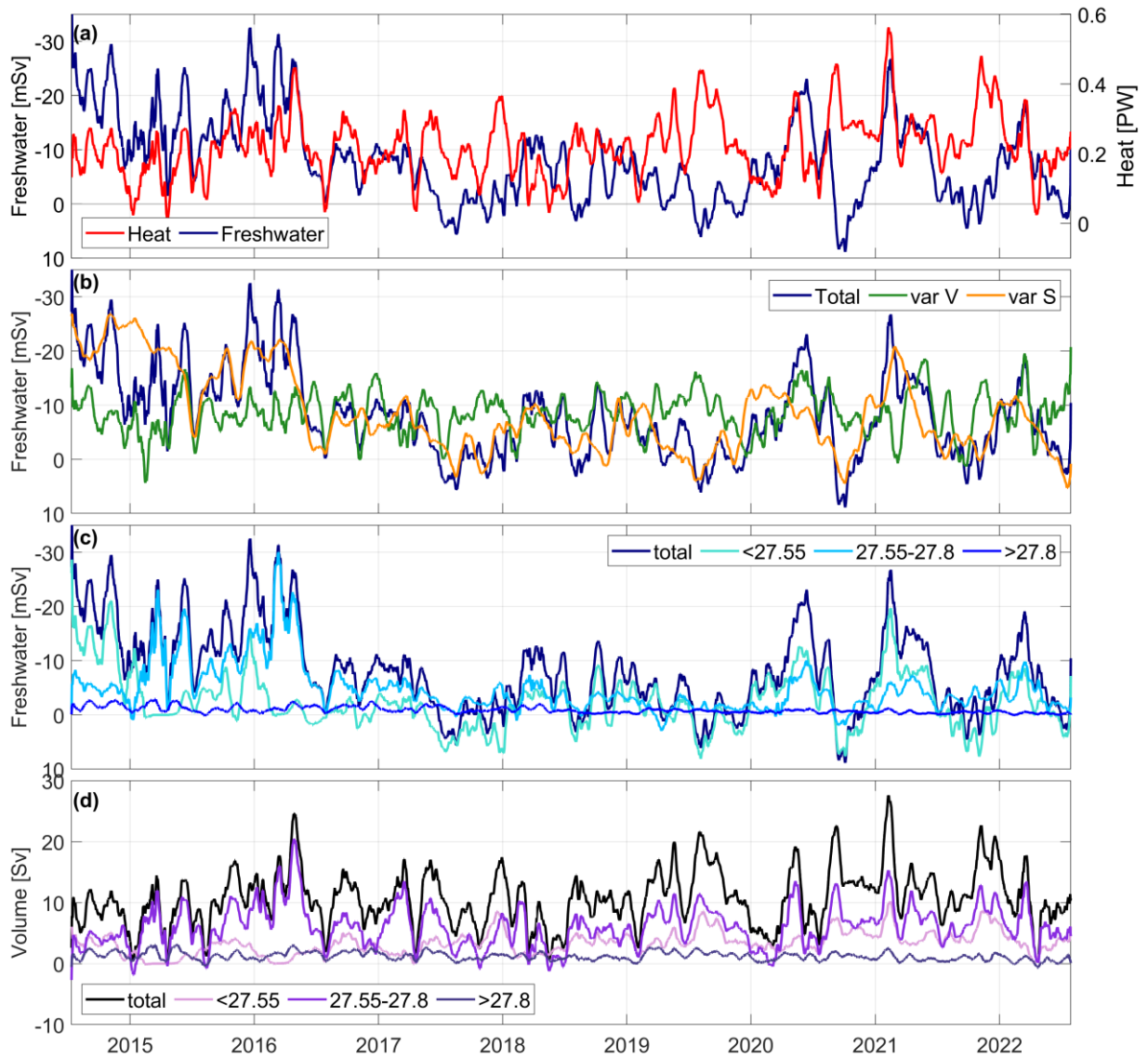


Figure 7: Transports of the Irminger Current Daily transport time series from IC mooring data smoothed by 30 days for 2014 – 2022 for (a) freshwater transport (blue, mSv) and heat transport (red, PW); note that the axis for freshwater transport reversed to represent northward salt transport; (b) total freshwater transport (total, blue), from constant salinity and variable velocity field (var V, green) and constant velocity and variable salinity field (var S, orange); (c) freshwater transport in density classes: total (dark blue, Sv), lighter than $\sigma_0 = -27.55 \text{ kg m}^{-3}$ -isopycnal (cyan), between $27.55 - 27.8 \text{ kg m}^{-3}$ (light blue) and denser than 27.8 kg m^{-3} (blue); (d) volume transport total (black, Sv), lighter than $\sigma_0 = 27.55 \text{ kg m}^{-3}$ - isopycnal (pink), between $27.55 - 27.8 \text{ kg m}^{-3}$ (purple) and denser than $\sigma_0 = 27.8 \text{ kg m}^{-3}$ (dark purple).

To investigate the relative importance of salinity versus velocity changes in the freshwater transport in a simplified way, we compute the freshwater transport from both the varying velocity and salinity field (Equation 3) with the other parameter kept at the record mean. In varS the salinity is varying as observed and the velocities are constant. In varV the salinity is kept constant, and the velocity is varying as observed. Figure 7b shows both constructed time series together with the actual total freshwater transport. The varS-time series nicely reproduces the actual freshwater transport on annual time scales or longer resulting in a moderate correlation to the total freshwater transport ($r=0.53$). Still the velocity field is

	14/15	15/16	16/17	17/18	18/19	19/20	20/21	21/22
--	-------	-------	-------	-------	-------	-------	-------	-------

responsible for variability on shorter time scales resulting in a similar moderate correlation ($r=0.59$). Overall, the freshwater transport is driven both by variations in the salinity and velocity field.

The influence of the velocity and/or salinity field on the freshwater transport can change over the water column. To assess the variability of freshwater transport more closely, we divide the freshwater transport up into three density classes: the upper water column (Layer 1: $\sigma_0 \leq 27.55 \text{ kg m}^{-3}$), the intermediate waters (Layer 2: $27.55 < \sigma_0 < 27.8 \text{ kg m}^{-3}$), and the deep overflow layer (Layer 3: $\sigma_0 \geq 27.8 \text{ kg m}^{-3}$; these isopycnals are marked in Figure 2, 3).

We show the respective effects of salinity and velocity on freshwater transport for each layer in Figure S1. The waters above the $\sigma_0 = 27.55 \text{ kg m}^{-3}$ - isopycnal (Layer 1, Fig.S1a) strongly correlate to the freshwater transport computed by a variable salinity field ($r=0.6$). The correlation to the varying velocity field is slightly weaker ($r=0.54$). Changes in the freshwater transport in the upper most layer are therefore slightly more driven by changes in salinity. The waters between $27.55\text{-}27.8 \text{ kg m}^{-3}$ (Layer 2, Fig.S1b) still show a moderate correlation ($r=0.47$) to a varying salinity field, but the effect of changing velocity field dominates ($r=0.69$). The freshwater transport of the lowermost layers is mainly driven by the velocity field (Layer 3, Fig.S1c, $r=0.91$), but still experience a strong influence from the salinity field ($r=0.5$). At depth the overall trend is driven by salinity but shorter variability by velocity. Therefore, the relationship between salinity and freshwater transport is strongest in the uppermost layer that experienced strongest freshening. As the impact of the salinity anomaly decreases over depth the influence of the velocity field on the freshwater transport increases.

Freshwater [mSv]	-15.5 ± 17.7	-16.1 ± 14.8	-6.1 ± 8.4	-3.8 ± 9.9	-4.2 ± 8.3	-6.1 ± 11.1	-7.7 ± 12.2	-4.6 ± 10.7
F < 27.55 kg m³	-6.4 ± 9.5	-3.0 ± 6.5	-0.2 ± 5.1	0.2 ± 6.5	-1.6 ± 6.4	-2.6 ± 7.6	-4.3 ± 9.3	-0.4 ± 7.9
27.55 < F < 27.8	-7.4 ± 14.1	-12.0 ± 12.2	-4.6 ± 4.7	-3.1 ± 5.3	-1.9 ± 3.3	-2.9 ± 5.0	-2.9 ± 4.0	-3.7 ± 4.2
F > 27.8 kg m³	-1.6 ± 1.5	-1.1 ± 1.1	-1.3 ± 1.2	-0.9 ± 1.0	-0.6 ± 0.6	-0.6 ± 0.6	-0.5 ± 0.5	-0.4 ± 0.5
Heat [PW]	0.17 ± 0.17	0.23 ± 0.18	0.21 ± 0.15	0.17 ± 0.16	0.22 ± 0.14	0.22 ± 0.17	0.29 ± 0.15	0.25 ± 0.17
Volume V [Sv]	8.3 ± 8.5	11.7 ± 9.4	10.8 ± 7.8	7.8 ± 8.2	11.2 ± 7.2	10.4 ± 8.6	13.9 ± 7.7	11.7 ± 8.8
V < 27.55 kg m³	1.7 ± 2.3 (21%)	2.0 ± 1.9 (17%)	2.8 ± 2.3 (25)	3.3 ± 2.7 (42%)	3.7 ± 2.4 (33%)	3.8 ± 2.9 (36%)	5.1 ± 2.8 (37%)	4.2 ± 3.1 (36%)
27.55 < V < 27.8	5.0 ± 7.4 (60%)	8.3 ± 8.3 (71%)	6.5 ± 5.9 (60%)	3.5 ± 6.2 (45%)	6.2 ± 4.8 (55%)	5.5 ± 6.1 (53%)	7.7 ± 5.1 (55%)	6.7 ± 6.1 (58%)
V > 27.8 kg m³	1.6 ± 1.6 (19%)	1.4 ± 1.3 (12%)	1.5 ± 1.4 (15)	1.0 ± 1.1 (13%)	1.3 ± 1.3 (12%)	1.2 ± 1.2 (11%)	1.1 ± 1.0 (8%)	0.7 ± 1.2 (6%)

Table 1: yearly mean values for freshwater, heat and volume transport from daily time

series First row: Total freshwater transport with corresponding standard deviation [mSv] together with freshwater transport split into density layers. Second row: Heat transport [PW]. Third row: Total volume transport [Sv] and split into density classes; numbers in brackets denote the percentage from the total transport.

To investigate the contribution of each layer to the total freshwater transport and possible changes, we show the respective freshwater transport time series per layer in Figure 7c. Before the arrival of the salinity the anomaly the upper and intermediate layer both equally contribute to the total freshwater transport (-6.4 mSv, -7.4 mSv respectively). Between 2016-2018, at the maximum strength of the salinity anomaly, the contribution drastically changes. In 2017-2018, the upper layer brings freshwater northward (+0.2 mSv) instead of salt. The intermediate layer changed to -3.1 mSv. The upper layer increased in salinity until a second drop in 2021/2022. The intermediate layer slowly recovers from the salinity anomaly. As most changes happen in the upper layer, its correlation to the total freshwater transport is strongest. Even though the deepest layer was least affected by the salinity anomaly, we find a long-term trend of decreasing northward salt transport.

To investigate possible changes for the AMOC's upper limb, we assess the impact of changes in freshwater transport on the volume transport. We correlate each layer of volume transport with its corresponding layer of freshwater transport (Fig.7c, d). The lower the correlation, the stronger changes in freshwater transport can be related to changes in salinity rather than changes in the volume transport. The freshwater transport of the upper layer, that experienced strongest changes in salinity, is weakly anti-correlated to its corresponding layer of volume transport ($r=-0.12$). The low correlation here again highlights that salinity is driving the changes in freshwater. Instead, the freshwater transport for the intermediate layer is weakly but significantly anticorrelated to the intermediate layer of volume transport ($r=-0.35$). As shown before this layer does experience a stronger contribution from the varying velocity field. The negative correlation arises from the fact that an increase in volume transport leads to a decrease in freshwater transport (= increase in salinity).

To highlight the major changes in the upper layers, we now investigate the respective contribution of each layer of volume transport to the total transport. The total volume transport increased from 8.3 Sv to 11.7 Sv with strong year-to-year variability (Tab.1). Before the anomaly, the upper layer only contributed with 1.7 Sv to the total transport. During the anomaly upper and intermediate layer nearly equally contribute to the total transport (3.3 Sv and 3.5 Sv in 2017-2018). The contribution of the upper layer stays high until the end of the record with 4.2 Sv. The contribution of the deepest layer decreases in response to the freshening. Even though we find strong variations in the total transport, the upper layer transport strongly increased, which potentially strengthens the upper limb.

In summary, the decrease in northward salt transport (increase in freshwater transport) changed the volume transport composition of the IC to a stronger contribution of lighter waters.

Discussion & Conclusion

In this study, we investigated the imprint of the recent freshwater anomaly described by Holliday et al. (2020) on salinity changes over the whole water column of the IC using high-resolution mooring data from 2014-2022. To put our results into a basin wide context, we combined this data set with hydrographic sections of the Irminger Sea and the Iceland Basin. At the IC array, the freshwater anomaly decreased the salinity over the entire upper 1500 m. Therefore, the freshwater anomaly should no longer be seen as a near surface anomaly. In response, the northward freshwater transport of the IC changed from -15.5 mSv in 2014-2015 to -4.6 mSv in 2021-2022. This indicates a decreasing northward salt transport; the IC's salinity gets closer to the used reference salinity. We could attribute the changes in freshwater transport in the upper layer to the salinity changes, rather than to volume transport changes. Previous studies showed that the salinity anomaly reached the Irminger Sea from the Iceland Basin (Biló et al., 2022; Devana et al., 2021). Concerning the onset of the upper ocean salinity anomaly, Devana et al. (2021) find low salinity waters in the upper 300m in the eastern Iceland Basin in autumn 2015. They further find that the anomaly reached the eastern flank of the Reykjanes Ridge by summer 2016 which agrees with our results on the western side of the ridge (Fig.2). We performed a lead-lag correlation between the mean salinity anomaly at 300-500 m for IC4 and M1. The highest correlation is at lag zero ($r = 0.78$) which highlights the strong and fast connection of the upper layers across the Reykjanes Ridge. We further investigated the recent salinity anomaly using hydrographic sections and find that the salinity anomaly extends across the Irminger Sea. By summer 2022, an oxygen sections reveals that waters with the same oxygen levels and low in salinity spread out from the central Irminger Sea (Fig.8). The high oxygen waters are freshly ventilated in the Irminger Sea, indicating that convection mixed the initial upper ocean fresh anomaly into the deeper layers of the water column. This deep pathway towards the IC likely explains the delayed and diluted freshening signal in the deeper part of the water column. Additionally, the freshening at depth could be advected from the Iceland Basin entering the Irminger Sea through Bight Fracture Zone. Devana et al. (2021) studied the mixing of the salinity anomaly into the Iceland Scotland Overflow Water in the Iceland Basin. They state that the salinity changes in the overflow plume are directly related to changes in the upper ocean through entrainment. Deep waters that got freshened in the Iceland Basin through this mechanism would arrive at the IC array much later than surface waters.

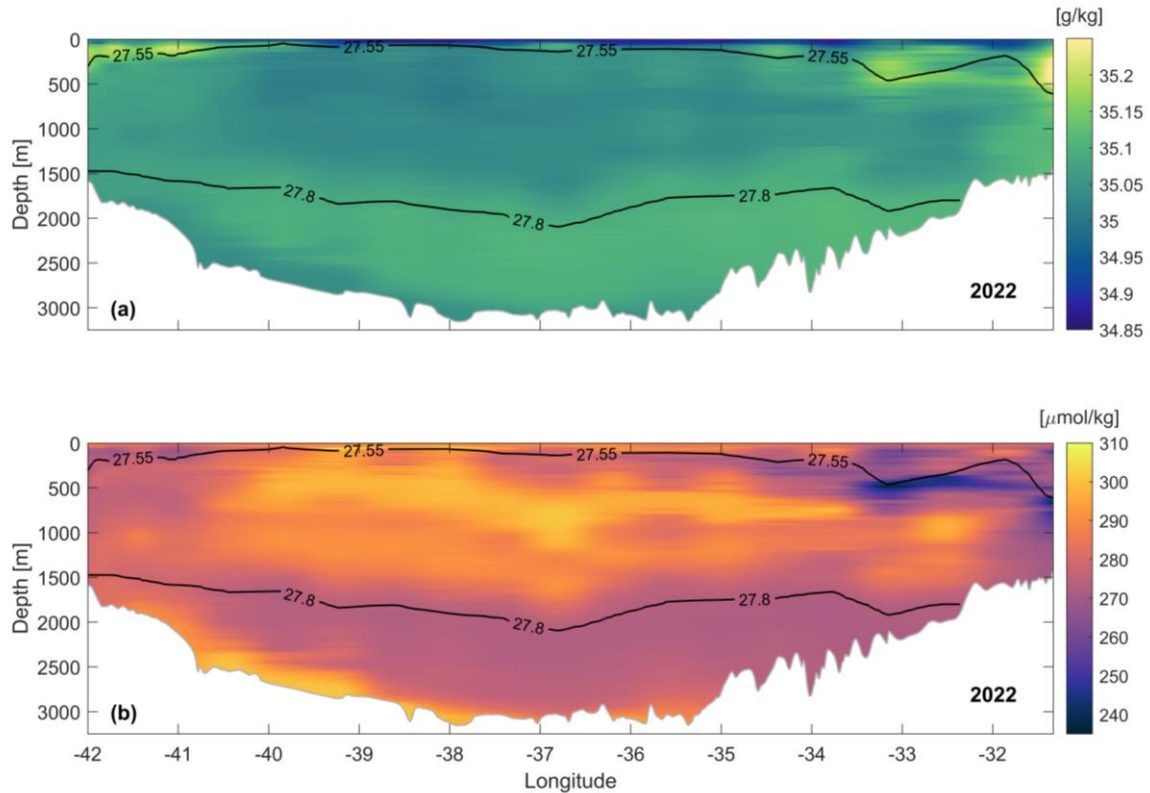


Figure 8: Salinity and Oxygen Section at OSNAP East for the Irminger Sea from 2022

(a) Salinity across the Irminger Sea from a hydrographic ship section in summer 2022 (shading) overlaid with isopycnals; (b) same as (a) but for oxygen.

By construction, our results are limited to the location of the IC moorings and only refer to the IC changes at OSNAP East. Deep waters from the Iceland Basin enter the Irminger Sea through various fractures zones in the Reykjanes Ridge (Fried et al., 2023; Koman et al., 2020; Petit et al., 2018). As the IC is constantly fed by waters from the Iceland Basin north of the OSNAP East section (Koman et al., 2020), it is likely that the upper waters of the IC downstream of OSNAP East experienced an earlier surface freshening. Mostly surface waters have the potential to cross westward into the Irminger Sea as the ridge is less deep north of the OSNAP East line. Overflow waters mostly enter the Irminger Sea through Bight Fracture Zone (Bower et al., 2019; Kanzow and Zenk, 2014; Petit et al., 2018; Zou and Lozier, 2017). The important pathway for the first onset of the salinity anomaly in the Irminger Sea are the surface waters crossing north of OSNAP East as the deep waters experienced the salinity anomaly later. The exact pathways of the anomaly entering the Irminger Sea are beyond the scope of this study.

Using a combination of hydrographic ocean analysis and mooring data Biló et al. (2022) show that the surface anomaly freshened the upper Irminger Sea waters to values as fresh as in the early 1990's. Our results show that indeed water across the whole basin reached low salinities as in the 1990's through the entire water column despite slightly warmer. At the IC array, waters below 500 m are even fresher than in 1992. We conclude therefore that the IC is in its freshest state observed since the 1990's.

In Fried and de Jong (2022), we showed that the basin-wide density gradient influences the transport variability at the IC array. We used 28 years of monthly reanalysis data to show that the increased volume transport during the 1990's was driven by a strong density gradient between the central Irminger Sea and the top of the Reykjanes Ridge. When the gradient was weak instead, around 2010/2011, the IC reached its lowest volume transport. We concluded that changes in the density gradient across the Irminger Sea can impact the volume transport at the IC array. A freshening of central Irminger Sea, as observed in this study, increases the density gradient between the interior and the IC and might explain the stronger volume transport observed in 2020-2021. At this point, the salinity anomaly on top of the ridge weakened while the interior Irminger Sea still freshened, increasing the contrast between fresher waters in the Irminger Sea and higher salinity on top of the ridge. But the intensity of the total transport also strongly depends on whether the mooring array captures the entire northward flow of the IC. Especially its western core is very variable in location and has therefore the potential to strongly impact the transport. A strong transport event can therefore also be caused by the western core being fully captured by the western most mooring. In addition, Fried and de Jong (2022) showed that the transport can also be influenced by mesoscale variability within the mooring array. Basin-wide observations in the Irminger Sea therefore remain crucial to understand and disentangle the mechanisms driving the transport variability of the IC.

In this study, we find that the volume transport of lighter waters ($\sigma < 27.55 \text{ kg m}^{-3}$) strongly increased due to the freshening of the waters above. In 2014-2015, the waters lighter than 27.55 kg m^{-3} contributed with 1.7 Sv to the total transport. By 2021-2022, this increased to 4.2 Sv. Therefore, the contribution of lighter waters to the total transport increased. The transport of intermediate waters is comparable at the beginning and at the end of the record. The overall increase in volume transport is likely a combination of the increased transport in the upper layers and the changing velocity structure of the IC. Specifically, the location of the IC's western core moved further east throughout the observed time period. De Jong et al.

(2020) showed that the western core is dominating the variability of the total volume transport, mostly due to its strong spatial variability.

In this study, we showed that the warm and saline IC drastically freshened in response to the most recent salinity anomaly resulting in an increase in the northward transport of lighter and fresher waters. The constant freshening of the AMOC's upper limb has the potential to suppress convection downstream in the Irminger Sea as well as in the Labrador Sea. However, once these freshwater anomalies are distributed over a large part of the water column the impact on stratification decreases. Therefore, monitoring and understanding the evolution of transient freshwater anomalies remains important to understand AMOC variability.

Acknowledgements

We thank all scientists and mariners involved in the OSNAP project who went to sea to collect the observational data used in this study. This project was funded by the European Union seventh Framework Program (FP7 2007–2013) under Grant 308299 (NACLIM), Horizon 2020 Research and Innovation Program under Grant 727852 (Blue-Action), the Innovational Research Incentives Scheme of the Netherlands Organization for Scientific Research (NWO) under Grant 016.Vidi.189.130, and the Royal Netherlands Institute for Sea Research. T. C. B. acknowledges the funding from the National Science Foundation under grant OCE1948198 and the NOAA's Global Ocean Monitoring and Observing program (FundRef number 100007298); NOAA's Climate Program Office, Climate Observations and Monitoring, and Climate Variability and Predictability programs under NOFO NOAA-OAR-CPO-2021-2006389 with additional NOAA Atlantic Oceanographic and Meteorological Laboratory support. Support for oxygen analysis for the 2022 section was provided by the U.S. National Science Foundation (OCE-1947970 to H. I. P.). This research was carried out in part under the auspices of the Cooperative Institute for Marine and Atmospheric Studies, a cooperative institute of the University of Miami and the National Oceanic and Atmospheric Administration (NOAA), cooperative agreement NA 20OAR4320472.

Open Research

We used mooring data from 2014 – 2022 from five deployments that are publicly available per deployment under:

de Steur, L., and M.F. de Jong (2018). High-resolution current meter and hydrographic data from the Irminger Current mooring array 2014-2015. NIOZ Royal Netherlands Institute for Sea Research. Dataset. <https://doi.org/10.4121/uuid:77b2c4fc-c253-4494-91bd-8d1ef66a014a>

de Steur, L., and M.F. de Jong (2018). High-resolution current meter and hydrographic data from the Irminger Current mooring array 2015-2016. NIOZ Royal Institute for Sea Research. Dataset. <https://doi.org/10.4121/uuid:9ae97ceb-39e4-43ec-abdb-614103285c16>

de Jong, M. F., and N. Fried (2021). "High-resolution current meter and hydrographic data from the Irminger Current mooring array 2016 - 2018", <https://doi.org/10.25850/nioz/7b.b.nb>

de Jong, M. F., and N. Fried (2021). "High-resolution current meter and hydrographic data from the Irminger Current mooring array 2018 - 2020", <https://doi.org/10.25850/nioz/7b.b.pb>

de Jong, M. F., and N. Fried (2024). "High-resolution current meter and hydrographic data from the Irminger Current mooring array 2020 - 2022", <https://doi.org/10.25850/nioz/7b.b.af>

In this study we used the gridded field for the entire time period 2014 – 2022 that has been published under:

de Jong, M.F., and N. Fried (2024). “Gridded high-resolution current meter and hydrographic data from the Irminger Current mooring array from 2014 – 2022”,
<https://doi.org/10.25850/nioz/7b.b.0f>

In addition, we used hydrographic sections from 1990 – 2022.
From 1990 – 2004 the near-annual surveys of the AR7 hydrographic section can be downloaded via <http://cchdo.ucsd.edu/>.

The OVIDE sections from 2002, 2004, 2006, 2008 and 2010 are available under:
Daniault Nathalie, Mercier Herle, Lherminier Pascale (2016). Gridded property and transport data of the biennial Greenland-Portugal A25 OVIDE line. SEANOE.
<https://doi.org/10.17882/46446>

The section data from 2014 – 2022 made freely available by the OSNAP (Overturning in the Subpolar North Atlantic Program) project and all the national programs that contribute to it (www.o-snap.org).

The 2015 OSNAP section data is available at <https://www.seanoe.org/data/00481/59302/> (de Jong & de Steur, 2019).

The 2020 OSNAP data is available
<https://dataverse.nioz.nl/dataset.xhtml?persistentId=doi:10.25850/nioz/7b.b.1f>
(de Jong, 2023).

The 2022 OSNAP section data is available at <https://cchdo.ucsd.edu/cruise/33VB20220819>
(Straneo, 2023). The calibrated oxygen data from this section will be available at BCO-DMO, under project “Collaborative Research: Gases in the Overturning and Horizontal circulation of the Subpolar North Atlantic Program (GOHSNAP)”: <https://www.bco-dmo.org/project/897705>.

References

- van Aken, H. M., & De Boer, C. J. (1995). On the synoptic hydrography of intermediate and deep water masses in the Iceland Basin. *Deep Sea Research Part I: Oceanographic Research Papers*, 42(2), 165-189.
- van Aken, H. M., de Jong, M. F., & Yashayaev, I. (2011). Decadal and multi-decadal variability of Labrador Sea Water in the north-western North Atlantic Ocean derived from tracer distributions: Heat budget, ventilation, and advection. *Deep Sea Research Part I: Oceanographic Research Papers*, 58(5), 505-523.
- Belkin, I. M., Levitus, S., Antonov, J., & Malmberg, S. A. (1998). “Great salinity anomalies” in the North Atlantic. *Progress in Oceanography*, 41(1), 1-68.
- Belkin, I. M. (2004). Propagation of the “Great Salinity Anomaly” of the 1990s around the northern North Atlantic. *Geophysical Research Letters*, 31(8).
- Biló, T. C., Straneo, F., Holte, J., & Le Bras, I. A. (2022). Arrival of New great salinity anomaly weakens convection in the Irminger Sea. *Geophysical Research Letters*, 49(11), e2022GL098857.
- Bower, A., Lozier, S., Biastoch, A., Drouin, K., Foukal, N., Furey, H., ... & Zou, S. (2019). Lagrangian views of the pathways of the Atlantic Meridional Overturning Circulation. *Journal of Geophysical Research: Oceans*, 124(8), 5313-5335.
- Chafik, L., Rossby, T., & Schrum, C. (2014). On the spatial structure and temporal variability of poleward transport between Scotland and Greenland. *Journal of Geophysical Research: Oceans*, 119(2), 824-841.
- Chafik, L., & Holliday, N. P. (2022). Rapid communication of upper-ocean salinity anomaly to deep waters of the Iceland Basin indicates an AMOC short-cut. *Geophysical Research Letters*, 49(3), e2021GL097570.
- Devana, M. S., Johns, W. E., Houk, A., & Zou, S. (2021). Rapid freshening of Iceland Scotland overflow water driven by entrainment of a major upper ocean salinity anomaly. *Geophysical research letters*, 48(22), e2021GL094396.
- Daniault, N., Mercier, H., Lherminier, P., Sarafanov, A., Falina, A., Zunino, P., ... & Gladyshev, S. (2016). The northern North Atlantic Ocean mean circulation in the early 21st century. *Progress in Oceanography*, 146, 142-158.
- Dickson, R. R., Meincke, J., Malmberg, S. A., & Lee, A. J. (1988). The “great salinity anomaly” in the northern North Atlantic 1968–1982. *Progress in Oceanography*, 20(2), 103-151.
- Eldevik, T., Straneo, F., Sandø, A. B., & Furevik, T. (2005). Pathways and export of Greenland Sea Water. In: *The Nordic Seas: an integrated perspective*.
- Fan, X., Send, U., Testor, P., Karstensen, J., & Lherminier, P. (2013). Observations of Irminger Sea anticyclonic eddies. *Journal of Physical Oceanography*, 43(4), 805-823.
- Fried, N., & de Jong, M. F. (2022). The role of the Irminger Current in the Irminger Sea northward transport variability. *Journal of Geophysical Research: Oceans*, 127(3), e2021JC018188.
- Fried, N., Katsman, C. A., & de Jong, M. F. (2023). Where do the two cores of the Irminger Current come from? A Lagrangian study using a 1/10 degree ocean model simulation. *Authorea Preprints*.

- Fox-Kemper, B., Hewitt, H. T., Xiao, C., Aðalgeirsdóttir, G., Drijfhout, S. S., Edwards, T. L., ... & Yu, Y. (2021). Ocean, cryosphere, and sea level change. In *Climate Change 2021: The Physical Science Basis. Contribution of Working Group I to the Sixth Assessment Report of the Intergovernmental Panel on Climate Change* (pp. 1211-1361). Cambridge University Press.
- Fu, Y., Lozier, M. S., Biló, T. C., Bower, A. S., Cunningham, S. A., Cyr, F., ... & Yashayaev, I. (2023). Seasonality of the Meridional Overturning Circulation in the subpolar North Atlantic. *Communications earth & environment*, 4(1), 181.
- Gelderloos, R., Straneo, F., & Katsman, C. A. (2012). Mechanisms behind the temporary shutdown of deep convection in the Labrador Sea: Lessons from the Great Salinity Anomaly years 1968–71. *Journal of Climate*, 25(19), 6743-6755.
- Holliday, N. P., Hughes, S. L., Bacon, S., Beszczynska-Möller, A., Hansen, B., Lavin, A., ... & Walczowski, W. (2008). Reversal of the 1960s to 1990s freshening trend in the northeast North Atlantic and Nordic Seas. *Geophysical Research Letters*, 35(3).
- Holliday, N. P., Bersch, M., Berx, B., Chafik, L., Cunningham, S., Florindo-López, C., ... & Yashayaev, I. (2020). Ocean circulation causes the largest freshening event for 120 years in eastern subpolar North Atlantic. *Nature communications*, 11(1), 585.
- Jackson, L.C. and R.A. Wood, 2018: Timescales of AMOC decline in response to fresh water forcing. *Climate Dynamics*, 51(4), 1333–1350, doi: 10.1007/s00382-017-3957-6.
- Jackson, L. C., Alastrué de Asenjo, E., Bellomo, K., Danabasoglu, G., Haak, H., Hu, A., Jungclaus, J., Lee, W., Meccia, V. L., Saenko, O., Shao, A., and Swingedouw, D.: Understanding AMOC stability: the North Atlantic Hosing Model Intercomparison Project, *Geosci. Model Dev.*, 16, 1975–1995, <https://doi.org/10.5194/gmd-16-1975-2023>, 2023.
- Johns, W. E., Devana, M., Houk, A., & Zou, S. (2021). Moored observations of the Iceland-Scotland overflow plume along the eastern flank of the Reykjanes Ridge. *Journal of Geophysical Research: Oceans*, 126(8), e2021JC017524.
- de Jong, M. F., van Aken, H. M., Våge, K., & Pickart, R. S. (2012). Convective mixing in the central Irminger Sea: 2002–2010. *Deep Sea Research Part I: Oceanographic Research Papers*, 63, 36-51.
- de Jong, M. F., & de Steur, L. (2016). Strong winter cooling over the Irminger Sea in winter 2014–2015, exceptional deep convection, and the emergence of anomalously low SST. *Geophysical Research Letters*, 43(13), 7106-7113.
- de Jong, M. F., Oltmanns, M., Karstensen, J., & de Steur, L. (2018). Deep convection in the Irminger Sea observed with a dense mooring array. *Oceanography*, 31(1), 50-59.
- de Jong, M. F., de Steur, L., Fried, N., Bol, R., & Kritsotakis, S. (2020). Year-round measurements of the Irminger Current: Variability of a two-core current system observed in 2014–2016. *Journal of Geophysical Research: Oceans*, 125(10), e2020JC016193.
- de Jong, M. F., Fogaren, K. E., Le Bras, I. A. A., McRaven, L. T., & Palevsky, H. I. (2023). Convection in the central Irminger Sea; insights into variability and the roles of surface forcing and stratification from 19 years of high resolution mooring data. *Authorea Preprints*.
- Jutras, M., Dufour, C. O., Mucci, A., & Talbot, L. C. (2023). Large-scale control of the retroflexion of the Labrador Current. *Nature Communications*, 14(1), 2623.

- Kanzow, T., & Zenk, W. (2014). Structure and transport of the Iceland Scotland Overflow plume along the Reykjanes Ridge in the Iceland Basin. *Deep Sea Research Part I: Oceanographic Research Papers*, 86, 82-93.
- Kim, W. M., Yeager, S., & Danabasoglu, G. (2021). Revisiting the causal connection between the great salinity anomaly of the 1970s and the shutdown of Labrador Sea deep convection. *Journal of Climate*, 34(2), 675-696.
- Knutsen, Ø., Svendsen, H., Østerhus, S., Rossby, T., & Hansen, B. (2005). Direct measurements of the mean flow and eddy kinetic energy structure of the upper ocean circulation in the NE Atlantic. *Geophysical Research Letters*, 32, L14604. <https://doi.org/10.1029/2005GL023615>
- Koman, G., Johns, W. E., & Houk, A. (2020). Transport and evolution of the East Reykjanes Ridge current. *Journal of Geophysical Research: Oceans*, 125(10), e2020JC016377.
- Lazier, J. R. (1973, April). The renewal of Labrador Sea water. In *Deep Sea Research and oceanographic abstracts* (Vol. 20, No. 4, pp. 341-353). Elsevier.
- Lazier, J. R. (1980). Oceanographic conditions at ocean weather ship Bravo, 1964–1974. *Atmosphere-ocean*, 18(3), 227-238.
- Lazier, J., Pickart, R., & Rhines, P. (2001). Deep convection. *International Geophysics*, 77, 387-400.
- Lherminier, P., Mercier, H., Gourcuff, C., Alvarez, M., Bacon, S., & Kermabon, C. (2007). Transports across the 2002 Greenland-Portugal Ovide section and comparison with 1997. *Journal of Geophysical Research: Oceans*, 112(C7).
- Li, F., Lozier, M. S., Bacon, S., Bower, A. S., Cunningham, S. A., De Jong, M. F., ... & Zhou, C. (2021). Subpolar North Atlantic western boundary density anomalies and the Meridional Overturning Circulation. *Nature communications*, 12(1), 3002.
- Lozier, M.S., Bacon, S., Bower, A. S., Cunningham, S. A., de Jong, F.M., de Steur, L., deYoung, B., Fischer, J., Gary, S. F., Greenan, B. J. W., Heimbach, P., Holliday, N. P., Houpert, L., Inall, M. E., Johns, W. E., Johnson, H. L., Karstensen, J., Li, F., Lin, X., Mackay, N., Marshall, D. P., Mercier, H., Myers, P. G., Pickart, R. S., Pillar, H. R., Straneo, F., Thierry, V., Weller, R. A., Williams, R. G., Wilson, C., Yang, J., Zhao, J., & Zika, J. D. (2017). Overturning in the Subpolar North Atlantic Program: A New International Ocean Observing System, *Bulletin of the American Meteorological Society*, 98(4), 737-752. doi: <https://doi.org/10.1175/BAMS-D-16-0057.1>
- Lozier, M. S., Li, F., Bacon, S., Bahr, F., Bower, A. S., Cunningham, S. A., de Jong, M. F., de Steur, L., deYoung, B., Fischer, J., Gary, S. F., Greenan, B. J. W., Holliday, N. P., Houk, A., Houpert, L., Inall, M. E., Johns, W. E., Johnson, H. L., Johnson, C., ... Zhao, J. (2019). A sea change in our view of overturning in the subpolar North Atlantic. *Science*, 363(6426), 516–521. <https://doi.org/10.1126/science.aau6592>
- Marshall, J., & Schott, F. (1999). Open-ocean convection: Observations, theory, and models. *Reviews of geophysics*, 37(1), 1-64.
- McDougall, T. J., & Barker, P. M. (2011). Getting started with TEOS-10 and the Gibbs Seawater (GSW) oceanographic toolbox. *Scor/Iapso WG*, 127(532), 1-28.
- Mercier, H., Lherminier, P., Sarafanov, A., Gaillard, F., Daniault, N., Desbruyères, D., ... & Thierry, V. (2015). Variability of the meridional overturning circulation at the Greenland–Portugal OVIDE section from 1993 to 2010. *Progress in Oceanography*, 132, 250-261.

- Messias, M. J., Watson, A. J., Johannessen, T., Oliver, K. I. C., Olsson, K. A., Fogelqvist, E., ... & Ledwell, J. R. (2008). The Greenland Sea tracer experiment 1996–2002: Horizontal mixing and transport of Greenland Sea intermediate water. *Progress in Oceanography*, 78(1), 85–105.
- Petit, T., Mercier, H., & Thierry, V. (2018). First direct estimates of volume and water mass transports across the Reykjanes Ridge. *Journal of Geophysical Research: Oceans*, 123(9), 6703–6719.
- Petit, T., Mercier, H., & Thierry, V. (2019). New insight into the formation and evolution of the East Reykjanes Ridge Current and Irminger Current. *Journal of Geophysical Research: Oceans*, 124(12), 9171–9189.
- Pickart, R. S., Spall, M. A., Ribergaard, M. H., Moore, G. K., & Milliff, R. F. (2003). Deep convection in the Irminger Sea forced by the Greenland tip jet. *Nature*, 424(6945), 152–156.
- Pickart, R. S., & Spall, M. A. (2007). Impact of Labrador Sea convection on the North Atlantic meridional overturning circulation. *Journal of Physical Oceanography*, 37(9), 2207–2227.
- Piron, A., Thierry, V., Mercier, H., & Caniaux, G. (2016). Argo float observations of basin-scale deep convection in the Irminger sea during winter 2011–2012. *Deep Sea Research Part I: Oceanographic Research Papers*, 109, 76–90.
- Read, J. F. (2000). CONVEX-91: water masses and circulation of the Northeast Atlantic subpolar gyre. *Progress in Oceanography*, 48(4), 461–510.
- Sarafanov, A., Falina, A., Mercier, H., Sokov, A., Lherminier, P., Gourcuff, C., ... & Danialt, N. (2012). Mean full-depth summer circulation and transports at the northern periphery of the Atlantic Ocean in the 2000s. *Journal of Geophysical Research: Oceans*, 117(C1).
- Sterl, M. F., & de Jong, M. F. (2022). Restratification structure and processes in the Irminger Sea. *Journal of Geophysical Research: Oceans*, 127(12), e2022JC019126.
- Stouffer, R. J., and Coauthors, 2006: Investigating the Causes of the Response of the Thermohaline Circulation to Past and Future Climate Changes. *J. Climate*, 19, 1365–1387, <https://doi.org/10.1175/JCLI3689.1>.
- Thornalley, D. J., Oppo, D. W., Ortega, P., Robson, J. I., Brierley, C. M., Davis, R., ... & Keigwin, L. D. (2018). Anomalously weak Labrador Sea convection and Atlantic overturning during the past 150 years. *Nature*, 556(7700), 227–230.
- Våge, K., Pickart, R. S., Sarafanov, A., Knutsen, Ø., Mercier, H., Lherminier, P., ... & Bacon, S. (2011). The Irminger Gyre: Circulation, convection, and interannual variability. *Deep Sea Research Part I: Oceanographic Research Papers*, 58(5), 590–614.
- Våge, K., Moore, G. W. K., Jónsson, S., & Valdimarsson, H. (2015). Water mass transformation in the Iceland Sea. *Deep Sea Research Part I: Oceanographic Research Papers*, 101, 98–109.
- Yashayaev, I. (2007). Hydrographic changes in the Labrador Sea, 1960–2005. *Progress in Oceanography*, 73(3–4), 242–276.
- Yeager, S., & Danabasoglu, G. (2014). The origins of late-twentieth-century variations in the large-scale North Atlantic circulation. *Journal of Climate*, 27(9), 3222–3247.

901 Zou, S., Lozier, S., Zenk, W., Bower, A., & Johns, W. (2017). Observed and modeled
902 pathways of the Iceland Scotland Overflow Water in the eastern North Atlantic. *Progress in*
903 *Oceanography*, 159, 211-222.
904